Journal of Vacuum Science & Technology B
ACCEPTED MANUSCRIPT
This is the author's peer reviewed, accepted manuscript. However, the online version of record will be different from this version once it has been copyedited and typeset.
PLEASE CITE THIS ARTICLE AS DOI: 10.1116/6.0003510

Study of defects population and contaminations in silica/tantala coated mirrors

D. D'Ubaldo,[1,2] M. Sbroscia,[1,3] V.C.A. Ficca,[1] E. Stellino,[4] A. Pasqualetti,[5] D. Sentenac,[5] J. Gargiulo,[5] L. Francescon,[5] L. Pinard,[6] and E. Placidi[1,3]
[1)] *University of Rome Sapienza, Physics department, Piazzale Aldo Moro 5, 00185 Rome Italy*
[2)] *University of Padua, Physics department, Padua Italy*
[3)] *INFN sez. Rome, Piazzale Aldo Moro 5, 00185 Rome Italy*
[4)] *University of Rome Sapienza, department of Basic and Applied Sciences for Engineering, Piazzale Aldo Moro 5, 00185 Rome Italy*
[5)] *European Gravitational Observatory (EGO), Cascina, Italy*
[6)] *Laboratoire des Matériaux Avancés - IP2I, CNRS, Université de Lyon, Université Claude Bernard, Lyon 1, Villeurbanne, F-69622, France*

(*Electronic mail: ernesto.placidi@uniroma1.it)

(Dated: 28 March 2024)

This article presents a study on the performance degradation of amorphous silica mirrors coated with silica/tantala, commonly utilized in gravitational wave interferometry measurements. The primary objective is to understand the factors contributing to the reduced performance, specifically the heightened noise observed after prolonged use of the mirrors in a vacuum. In this article, SiO_2/Ta_2O_5 multilayered coated sample mirrors underwent analysis through X-ray photoemission spectro-microscopy, Atomic Force Microscopy, and Raman spectroscopy, before and after exposure to a contaminating vacuum environment. Our findings revealed the possible correlation between the deterioration in mirror performance and an upsurge in contaminant carbon and defect populations within the silicon dioxide structure.

I. INTRODUCTION

Gravitational-wave (GW) interferometers are at the forefront of experimental physics, employing optics of exceptional precision and unparalleled performance. The main optics typically have diameters up to 35 cm and mass about 40 kg, with a surface roughness of less than 1 nm and extremely low optical losses[1–3]. Even larger and more performant optics are considered for the upcoming upgrades of existing interferometers and for the next-generation detectors.[4,5] To minimize environmental disturbances that mask the very weak gravitational-wave signal, the entire detector, including the optics, operates under ultra-high vacuum. Stringent cleanliness is crucial, in order to prevent the deposition of low-volatile molecules present among the residual gas species. These molecules, outgassing from "contaminated" components within the vacuum environment, can accumulate on surfaces and form films thick enough to degrade optical properties, notably surface absorption and scattering. This issue is enhanced in GW research due to the length of experiments, which can last for months or years, increasing the sensitivity to even low levels of contaminants. Furthermore, the large size of vacuum chambers, exceeding 10 m^3, makes recovery from accidental contamination extremely difficult, necessitating a complete disassembly and cleaning. Careful selection on materials to be placed in the chambers near the optics is essential.[6,7] The current process for assessing material compatibility includes two complementary methods: vacuum testing to measure the outgassing of low-volatile species from the candidate material, and direct measurements of effects on optical properties. However, these methods often reveal inconsistencies, preventing the establishment of a clear correlation between the two.[8] To overcome these limitations, we propose a method using X-ray photoelectron spectroscopy (XPS) to directly analyze contamination on the test surfaces. This technique provides a direct and quantitative assessment of contamination on the surface.

II. MATERIALS AND METHODS

The experimental investigation was carried out on SiO_2/Ta_2O_5 oxide multilayer sample mirrors deposited by Ion Beam Sputtering (IBS) at the Laboratoire des Matériaux Avancés (Lyon, France). The thin films were composed of 20-25 alternating layers of SiO_2 and Ti:Ta_2O_5, with a thickness of each layer around 100 nm for high index layer and 200 nm for low index layer (multilayer design optimized to lower the coating thermal noise).

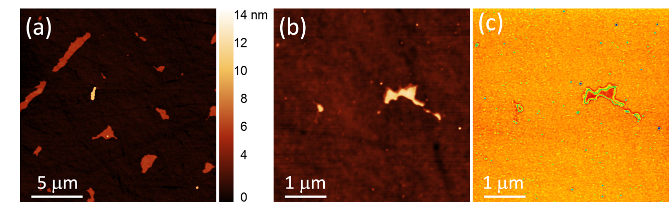

FIG. 1. (a) $20\times 20\,\mu m$ topography of contaminated SiO_2, (b) $5\times 5\,\mu m$ AFM topography of contaminated SiO_2 and (c) the corresponding phase image.

Each sample had a diameter of 1" and a thickness of 6 mm and was mounted onto an *ad-hoc* sample holder developed by us, which could be inserted in the Ultra-High-Vacuum (UHV) chamber to perform X-ray photoemission spectroscopy (XPS).
The measurements were carried out on two reference samples,

Journal of Vacuum Science & Technology B
ACCEPTED MANUSCRIPT
This is the author's peer reviewed, accepted manuscript. However, the online version of record will be different from this version once it has been copyedited and typeset.
PLEASE CITE THIS ARTICLE AS DOI: 10.1116/6.0003510
AVS

one contaminated and one clean. The contaminated sample underwent exposure for approximately 96 hours, maintained at a pressure of around 10^{-7} mbar within a specialized vacuum chamber where contaminating materials were present (fluorinated rubber, possibly containing additives such as molding agents, waxes, and flame retardants). During the contamination tests, the approach is to assess contamination risk by deliberately increasing exposure, bringing the potential contaminant and test surface closer than their typical real-life arrangement. The clean reference sample was a mirror that did not undergo any such treatment, i.e., exposed to the minimal handling required for its insertion into the XPS apparatus.
The XPS measurements were carried out using the SPECS XPS apparatus equipped with a flood gun SPECS FG 22, and proprietary SpecsLab Prodigy software for data acquisition and experiment control.
The XPS measurements were performed both with integrated signal and in microscopic analysis: a total surface of 1 cm^2 of the sample was divided into an array of 10x10 points, for a total of 100 measurement points.
Measurements on the contaminated sample were repeated after a mild Ar^+ sputtering for comparison. The sputtering was 30 minutes long at a current intensity of 10 mA, a voltage of 1.2 kV, and a pressure of 1.0×10^{-6} mbar, resulting in a controlled and localized removal of the surface layer of the sample by a flow of Ar particles with an estimated thickness of approximately 10 nm.

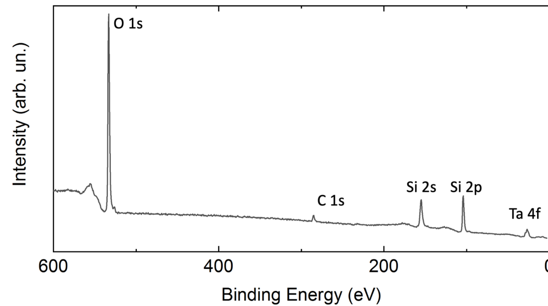

FIG. 2. Survey XPS spectrum of reference sample.

Due to the dielectric nature of the surface, during the measurements we employed a flood gun to compensate the positive spatial charge regions present on the sample surface generated by the outgoing photoelectrons.[9] A partial charge compensation was preferred to a complete: in fact, we sought the relative optimal measurement conditions to sufficiently compensate the charge present on the surface while limit spatial charge fluctuations on the surface[10] that occur when the electron flux increases. The optimized conditions were found with electrons accelerated by a potential of 1.5 V and a current of 70 μA. Measurements were carried out using an atomic force microscope (AFM) Park NX10. The AFM data were acquired through three different scanning areas of 50, 20, and 5 square micrometers, respectively. All scans were performed in Tapping mode using NCHR (Non-Contact High Resolution) probes to minimize the pressure exerted by the probe on the sample surface.
Raman measurements were carried out by a LabRam HR Evolution Horiba micro-spectrometer operating in backscattering geometry. A 532 nm solid-state laser was employed as a light source, coupled with a monochromator with 600 grooves/mm and a Peltier-cooled charge-coupled-device detector.[11] The elastic component of the scattered light was removed by a volume Bragg grating optical filter. Both AFM and Raman measurements were performed in air.
The AFM data was processed using Gwyddion 2.61 software,[12] while the XPS data was processed using KolXPD 1.8 software. The data presented in this study were collected by averaging three measurements taken at the same point on the array.
The relative area for each peak was calculated with respect to the signal of the measure's background. This ratio provides an adimensional value that describes the spectrum which can be compared with other spectra observed under the same experimental conditions. Voigtian curves were employed for data interpolation.

III. RESULTS

First, AFM topographies were acquired on both samples. While clean samples present a flat morphology with an RMS roughness of less than one nm, samples exposed to contaminants show the same morphology but with the presence of small structures with a surface density around $4\times10^{-6}\,cm^{-2}$, which extend planarly with a thickness between 1 and 4 nm. The phase imaging (Panel (c) in Fig 1) points out a contrast between the signal coming from the internal part of such structures and the substrate. Phase contrast is typically due to regions with different mechanical properties, this can be related to different material bonding or to adsorbate with different chemical nature. Since we found it only in some areas, we consider more probable the presence of some kind of adsorbate on the surface different from the coating (we don't take into account the bright contrast that is typically present on the structure edge).

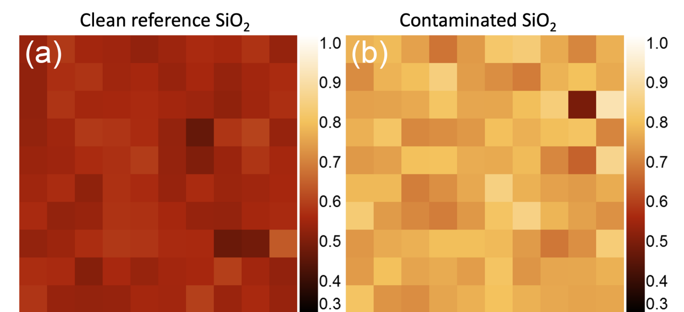

FIG. 3. 10×10 mm XPS normalized intensity maps of the C1s peak. The intensity is normalized with the signal background. (a) is the image of clean reference mirror, while (b) the contaminated one

ACCEPTED MANUSCRIPT
Journal of Vacuum Science & Technology B
This is the author's peer reviewed, accepted manuscript. However, the online version of record will be different from this version once it has been copyedited and typeset.
PLEASE CITE THIS ARTICLE AS DOI: 10.1116/6.0003510

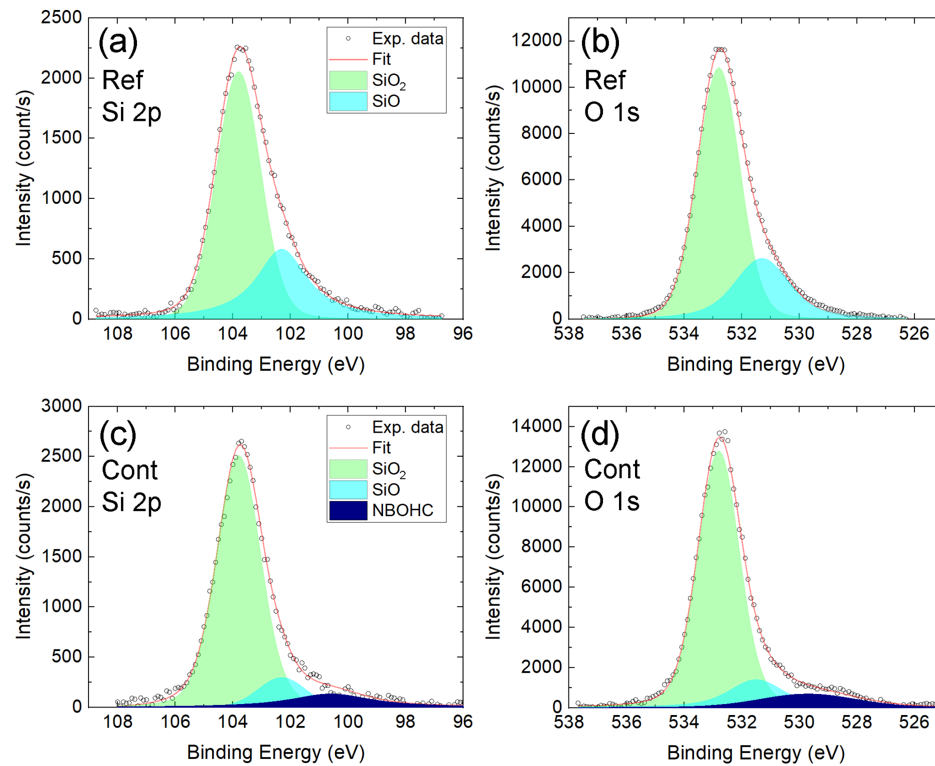

FIG. 4. Si2p and O1s peaks deconvolution for reference (a-b) and contaminated SiO_2 (c-d).

Figure 2 shows the XPS survey spectra of the two samples. The 1s peak of oxygen at binding energy around 532 eV is of course the most intense. Specifically, n the 100-150 eV range, 2s and 2p peaks of silicon are visible, while the peak at about 25 eV can be assigned to the 4f of tantalum, which probably emerges from a small tantala segregation during the silica deposition. The oxygen and silicon peaks are in the right stoichiometric ratio while the tantalum signal is very small because it comes from deeper layers. The only element that represents a contamination with respect to the ideal chemical structure of the mirror is carbon that exhibit a small C 1s peak at around 284 eV. This can be present on the surface in various forms, but we can exclude the presence of complex organic molecules (hydrocarbons). Indeed, although XPS cannot probe for the presence of hydrogen, Raman measurements have not identified the presence of any hydrocarbons, as will shown later in Fig. 5.

It is not completely clear if the structure observed with AFM are correlated to the higher presence of carbon on the surface. Indeed, the density of such stucture is rather low (In AFM images in Fig. 1 we detected an higher presence), so that probably the XPS signal related to those does not emerge from noise.

XPS intensity maps were generated mapping the ratio between C1s peak area in the range 280-290 eV and the background in the same range. XPS spectra were acquired in high spatial resolution taking the signal for an area less than 1 mm^2: a total surface of 1 cm^2 of the sample was divided into an array of 10x10 points, for a total of 100 measurement points.

Fig. 3(a-b) represents the comparison between the C1s intensity maps for clean and contaminated surface. As also observed for the integrated spectra, the average carbon signal in the maps for the contaminated mirrors is approximately 40% higher compared to the corresponding maps acquired in the clean sample. Furthermore, the RMS roughness (which, in this case, represents the fluctuation of the intensity of the signal) of the maps on the contaminated signal is around 45% higher than the corresponding measurement on the clean signal. This suggests not only an elevated presence of carbon on the surface but also a noteworthy increase in variability within the contaminated sample.

From the deconvolution of the line shapes of the Si2p and O1s peaks (Fig. 4), we observe the presence of two components for the signals relating to the reference sample and three peaks for the contaminated sample. In the contaminated sample we find the O1s components at 532.8, 531.5 and 529.7 eV. The first two peaks are also present in the reference sample, while the third is not. The same goes for the deconvolution of the Si2p peak, where the components at 103.8, 102.3 eV are present on both samples, while the component at 100.5 eV only in the contaminated sample.

The peak at 532.8 eV is characteristic of oxygen present in a silicon oxide matrix[13], just as the peak at 103.8 is characteristic of silicon in the SiO_2 crystal. The peak at 531.5 eV (and its counterpart at 102.3 for Si) is ascribed to the silanol group, whereas the component at 529.7 eV (with its equivalent at 100.5 for Si) is associated with non-bridging oxygen hole centers (NBOHC). These defects are commonly found in atoms/molecules bonded to a single atom, with the valence aiming to minimize the bond energy.[14–16].

ACCEPTED MANUSCRIPT
Journal of Vacuum Science & Technology B
This is the author's peer reviewed, accepted manuscript. However, the online version of record will be different from this version once it has been copyedited and typeset.
PLEASE CITE THIS ARTICLE AS DOI: 10.1116/6.0003510

The analysis of the spectra indicates that the peak related to silicon monoxide (SiO) is reduced in the presence of contamination and the appearance of the NBOHC peak is observed.

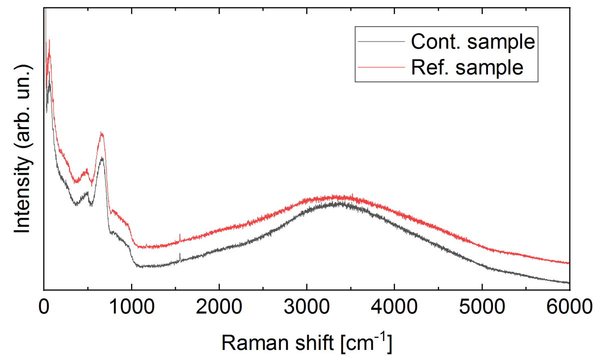

FIG. 5. Raman spectra for reference (black line) and contaminated (red line) mirrors.

The Raman spectra for reference and contaminated mirrors are shown in Fig. 5 and are characterized by the presence of a complex structure in the first 1000 cm^{-1} while a broad band can be noted in the second portion of the spectrum at (3000-4000 cm^{-1} range). The first band is associated to the photoluminescence characteristic of NBOHC silicon defects. Given the strong correspondence of the spectra, both samples were measured also on the amorphous silica of the opposite uncoated side (not shown). The comparison confirms that Raman spectra are practically identical for reference and contaminated sample apart a non-significative difference on the broad band centered around 3500 cm^{-1}.
The occurrence of typical NBOHC bands on both the samples testifies the presence of such defects in the bulk whose density is probably below the detection limit of XPS. Contaminating the sample likely increases the defect density on the surface, making possible their detection. Considering that the sampling depth decreases from the micron to the nanometer scale passing from Raman to XPS, the observation of discernible, albeit minor, changes in XPS spectra of the two samples, while the correspondent Raman spectra remain practically identical, indicates that any contamination likely resides exclusively on the surface and does not penetrate the mirrors.

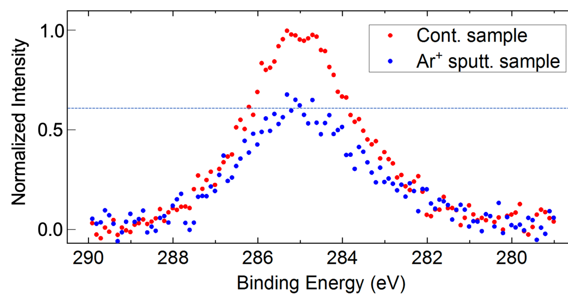

FIG. 6. C1s peak for the contaminated mirror acquired before (red dots) and after (blue dots) the Ar^+ ion bombardment. The dashed line is placed at the 0.6 value.

To quantify the contamination due to the carbon present on the surface, a light sputtering was carried out using Ar^+ ions (10 minutes at a pressure of 10^{-6} mbar and energy of 1.2 keV). The XPS spectra of C1s before and after ion bombardment are shown in Fig.6. It is observed that the C1s signal is reduced by approximately 40% compared to the contaminated sample, in agreement with the intensity observed in the reference sample. This further asserts that carbon contamination is due to weak carbon bound to the crystal surface. This is corroborated by the fact that subsequent sputtering did not lead to a further reduction in the C1s signal.

IV. CONCLUSIONS

Reference and high-vacuum contaminated SiO_2/Ta_2O_5 multilayer mirrors were characterized by AFM, XPS and Raman spectroscopy. The only contaminant detected in XPS appears to be carbon. In particular, the presence of non-adventitious surface carbon is confirmed both by the direct observation of planar structures on the surface with the AFM and by the increase in the carbon signal in XPS of the contaminated sample compared to the reference sample. Raman measurements confirms that the contamination is present only on the surface, as no signal difference is observed between the two samples. Finally appreciable difference is observed in the signal of the two samples: in the contaminated sample, a greater presence of non-bridging oxygen hole center defects is observed, which therefore appears correlated to the greater presence of carbon.

V. ACKNOWLEDGEMENTS

The integrated XPS and XPS maps were carried out at the SmartLab departmental laboratory of the Department of Physics at Sapienza University of Rome. The authors are grateful to Prof. P. Postorino for useful discussion and for the use of HPS laboratory. This work was supported by project 2020Y2JMP5 'ANDROMeDa' (CUP: I85F21004170005) funded by MUR PRIN 2020

VI. CONFLICT OF INTEREST

The authors have no conflicts to disclose.

VII. DATA AVAILABILITY

The data that support the findings of this study are available from the corresponding author upon reasonable request.

VIII. REFERENCES

[1] M. Acernese et al, "Advanced virgo: a second-generation interferometric gravitational wave detector," Classical and Quantum Gravity **32**, 024001 (2014).

Journal of Vacuum Science & Technology B
ACCEPTED MANUSCRIPT
This is the author's peer reviewed, accepted manuscript. However, the online version of record will be different from this version once it has been copyedited and typeset.
PLEASE CITE THIS ARTICLE AS DOI: 10.1116/6.0003510

[2] T. L. S. Collaboration, "Advanced ligo," Classical and Quantum Gravity **32**, 074001 (2015).

[3] T. Akutsu et al, "Kagra: 2.5 generation interferometric gravitational wave detector," Nature Astronomy **3**, 35–40 (2019).

[4] M. Punturo et al., "The einstein telescope: a third-generation gravitational wave observatory," Classical and Quantum Gravity **27**, 194002 (2010).

[5] R. Flaminio, "Status and plans of the virgo gravitational wave detector," SPIE Astronomical Telescopes + Instrumentation 2020, Online, United States. pp.1144511, 0.1117/12.2565418 hal-03107929 (2020).

[6] S. Tanioka, K. Hasegawa, and Y. Aso, "Optical loss study of molecular layer for a cryogenic interferometric gravitational-wave detector," Phys. Rev. D **102**, 022009 (2020).

[7] A. Gargiulo, J. Pasqualetti, D. Sentenac, and for the VAC team, "Advanced virgo technical design report," Virgo collaboration, "Advanced Virgo Technical Design Report" (2024).

[8] A. Gargiulo, J. Pasqualetti, D. Sentenac, and for the VAC team, "Synthesis of methods for in-vacuum contamination assessment and material selection for virgo towers," Virgo collaboration, "Advanced Virgo Technical Design Report" , VIR–0410A–22 (2024).

[9] A. Paolone, E. Placidi, E. Stellino, M. G. Betti, E. Majorana, C. Mariani, A. Nucara, O. Palumbo, P. Postorino, M. Sbroscia, F. Trequattrini, M. Granata, D. Hofman, C. Michel, L. Pinard, A. Lemaitre, N. Shcheblanov, G. Cagnoli, and F. Ricci, "Argon and other defects in amorphous sio2 coatings for gravitational-wave detectors," Coatings **12** (2022), 10.3390/coatings12071001.

[10] D. R. Baer, K. Artyushkova, H. Cohen, C. D. Easton, M. Engelhard, T. R. Gengenbach, G. Greczynski, P. Mack, D. J. Morgan, and A. Roberts, "XPS guide: Charge neutralization and binding energy referencing for insulating samples," Journal of Vacuum Science Technology A **38**, 031204 (2020), https://pubs.aip.org/avs/jva/article-pdf/doi/10.1116/6.0000057/15714286/031204_1_online.pdf.

[11] I. Pallecchi, E. Stellino, P. Postorino, A. Iyo, H. Ogino, M. Affronte, and M. Putti, "Experimental investigation of electronic interactions in collapsed and uncollapsed lafe$_2$as$_2$ phases," Phys. Rev. B **108**, 014512 (2023).

[12] D. Nečas and P. Klapetek, "Gwyddion: An open-source software for spm data analysis," Central European Journal of Physics **10** (2011), 10.2478/s11534-011-0096-2.

[13] A. K. Mishra, R. Belgamwar, R. Jana, A. Datta, and V. Polshettiwar, "Defects in nanosilica catalytically convert co₂ to methane without any metal and ligand," Proceedings of the National Academy of Sciences **117**, 6383–6390 (2020), https://www.pnas.org/doi/pdf/10.1073/pnas.1917237117.

[14] R. Bossoli, M. Jani, and L. Halliburton, "Radiation-induced e centers in crystalline sio2," Solid State Communications **44**, 213–217 (1982).

[15] L. Skuja, "The origin of the intrinsic 1.9 ev luminescence band in glassy sio2," Journal of Non-Crystalline Solids **179**, 51–69 (1994), proceedings of the First PAC RIM Meeting on Glass and Optical Materials.

[16] F. Messina, L. Vaccaro, and M. Cannas, "Generation and excitation of point defects in silica by synchrotron radiation above the absorption edge," Phys. Rev. B **81**, 035212 (2010).